Reflected Wave Modeling in Heterogeneous Acoustic Media Using the De Wolf Approximation

Ru-Shan Wu and Lian-Jie Huang

Institute of Tectonics, University of California

Santa Cruz, CA 95064, USA

Published in

Mathematical Methods in Geophysical Imaging III

Editor: Siamak Hassanzadeh

Proc. SPIE 2571, p176–186 (1995)

Reflected wave modeling in heterogeneous acoustic media using the De Wolf approximation

Ru-Shan Wu and Lian-Jie Huang

Institute of Tectonics, University of California, Santa Cruz, CA 95064, USA

ABSTRACT

A fast modeling method based on multiple-forescattering single-backscattering (MFSB) approximation, *i.e.* the De Wolf approximation for calculating reflected (or backscattered) wave fields in 3-D heterogeneous acoustic media is introduced. The method is much faster than full wave finite difference or finite element methods. The formulation is especially suitable for the configuration of surface reflection surveying. When discontinuities in a medium are not very sharp or parameter perturbations of heterogeneities are not very strong, reverberations between heterogeneities or resonance scattering can be neglected. However, for large volume heterogeneous media or long propagation distances the accumulated effect of multiple forward scattering becomes very important for both forward modeling and inverse problems. In such cases, the Born approximation is not valid while the De Wolf approximation can be applied. After renormalizing the multiple scattering series of the Lipmann-Schwinger equation, a MFSB approximation for acoustic waves is derived and a fast dual-domain computation scheme is presented, in which the multi-screen one-way wave propagator is used. Finally numerical examples are given to demonstrate the validity of the method.

Keywords: acoustic wave, backscattering, De Wolf approximation, modeling, thin-slab.

1 INTRODUCTION

Fast modeling methods and algorithms in complex heterogeneous media, especially for 3-D media, are crucial to the development of imaging and inversion methods, interpretations and applications of seismic methods for complex structures. Finite difference and finite element methods, which in principle can model wave propagation in arbitrarily heterogeneous media, are time consuming, even formidable in the case of large 3-D elastic wave problems. High-frequency asymptotic methods, such as ray methods can be used for the case of smoothly varying media (Červený,[2] 1981; Červený and Klimeš,[3] 1984; Chapman,[4] 1985). However, all the frequency-dependent and wave related phenomena in complex media can not be modeled by ray methods. Born scattering formulation (Gubernatis *et al.*,[9] 1977; Wu and Aki,[14] 1985), ray-Born (Beydoun and Mendes,[1] 1989; Coates and Chapman,[5] 1990), or generalized Born scattering (Coates and Chapman,[6] 1991) can model small volume complex heterogeneities in smooth background media. But they are not capable of modeling large volume or long distance propagation problems in complex media. It is necessary to develop intermediate modeling methods functioning between the full wave equation methods and the high-frequency asymptotic methods. For the modeling of backscattered fields of surface reflection surveying, reverberations between heterogeneities or resonance scattering can often be neglected. However, accumulated effects of forward scattering (or forescattering), such as the phase shift and wavefront distortion, focusing/defocusing, and multi-pathing, usually can not be neglected. In fact, for large volume heterogeneous media or long distance propagation, multiple forescattering is very important for both forward modeling and inverse problems. In this study we develop a new method based on multiple-forescattering single-backscattering (MFSB) approximation, *i.e.* the De Wolf approximation (De Wolf,[7, 8] 1971, 1985) for the modeling of reflected wave fields in the configuration of surface reflection surveying. A dual-domain formulation is derived for fast implementation of the method. The method retains the major features of full wave equation methods for most cases of practical applications, but has a much higher computation speed and less memory

requirement relative to full wave methods. Numerical examples are given to demonstrate the validity of the method. They demonstrate that the incidence angle dependence of reflected wave amplitudes by this numerical method matches well with theoretical predictions, including critical reflections, up to 70 degrees. Therefore, the wide-angle algorithm of the method could be used to model wide-angle reflected (backscattered) or transmitted (forescattered) acoustic waves. Approximations to this method, such as the screen approximation for the case of large scale heterogeneities, for further reducing the computation time, have been discussed by Wu *et al.*[16] (1995) and Xie and Wu[17] (1995). Detailed comparisons between different versions of the method and their accuracy analyses are left for future publications.

2 DE WOLF APPROXIMATION

2.1 Lipmann-Schwinger equation

The constant density scalar wave equation is

$$\left[\nabla^2 + \frac{\omega^2}{c^2(\mathbf{x})}\right] p(\mathbf{x}) = 0 \,. \tag{1}$$

Let $c_0(\mathbf{x})$ be the velocity of the background medium, then we have

$$\left(\nabla^2 + k^2\right) p(\mathbf{x}) = -k^2 F(\mathbf{x}) p(\mathbf{x}) \,, \tag{2}$$

where $k = \omega/c_0$ is the background wavenumber and

$$F(\mathbf{x}) = \frac{c_0^2}{c^2(\mathbf{x})} - 1 = \frac{s^2(\mathbf{x}) - s_0^2}{s_0^2} = \varepsilon(\mathbf{x}) \tag{3}$$

is the perturbation function (dimensionless force), in which $s = 1/c$ is the slowness of the medium. Let

$$p(\mathbf{x}) = p^0(\mathbf{x}) + P(\mathbf{x}) \,, \tag{4}$$

then we have

$$p(\mathbf{x}) = p^0(\mathbf{x}) + k^2 \int_v d^3\mathbf{x}' g(\mathbf{x};\mathbf{x}') F(\mathbf{x}') p(\mathbf{x}') \,, \tag{5}$$

where $g(\mathbf{x};\mathbf{x}')$ is the Green's function in the background medium. This is the Lipmann-Schwinger equation.

2.2 Renormalization of scattering series and the De Wolf approximation

The Lipmann-Schwinger equation (5) has a formal solution of multiple scattering Born series. The widely used Born approximation is the leading term of the series. The Born approximation is only valid when the heterogeneities are weak and the propagation distance is short. After renormalization of the multiple scattering series, De Wolf[7, 8] (1971, 1985) derived a MFSB approximation given by

$$p(\mathbf{x}) = p^f(\mathbf{x}) + k^2 \int_v d^3\mathbf{x}' g^f(\mathbf{x};\mathbf{x}') F(\mathbf{x}') p^f(\mathbf{x}') \,, \tag{6}$$

where p^f and g^f are the renormalized, multiple forescattered field and Green's function, respectively. In this paper, p^f and g^f will be calculated using the phase-screen propagator. Note that in the De Wolf approximation, both the total exact field and the free space Green's function are replaced by the renormalized, multiple forescattering approximations, and is superior to the approximations made by Wu and Huang[15] (1992) in which only the total exact field is approximated by p^f but the free space Green's function is left intact. This MFSB approximation is valid whenever the backscattered field is much smaller than the forescattered field.

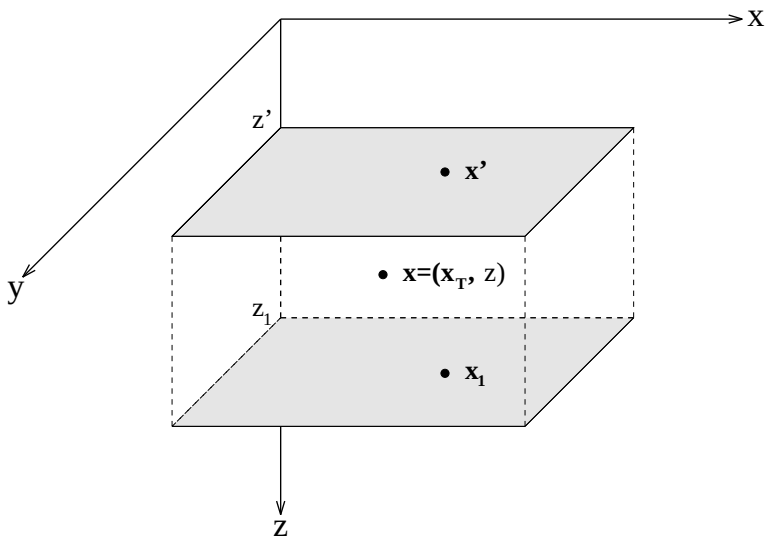

Figure 1: Illustration of a thin-slab.

2.3 Implementation of the MFSB synthetics by a dual-domain technique

The scattered field at a receiving point $(x_T^*,\ z^*)$ can be calculated using equation (6) as

$$P(\mathbf{x}_T^*, z^*) = k^2 \int_v d^3\mathbf{x} g^f(\mathbf{x}_T^*, z^*; \mathbf{x}) F(\mathbf{x}) p^f(\mathbf{x}) \ , \tag{7}$$

where $\mathbf{x}_T^*$ is the horizontal position in the receiver plane at depth z^*. Equation (7) can be numerically implemented using the phase-screen propagator (Thomson and Chapman,[12] 1983; Martin and Flatté,[10] 1988; Stoffa *et al.*,[11] 1990; Wu and Huang,[15] 1992; Wu,[13] 1994). To speed up the calculation of backscattered fields, the local Born approximation can be used within a thin-slab (*cf.* Figure 1). This means that the forescattered field p^f can be kept unperturbed and g^f can be replaced by a constant medium Green's function within the slab. Assume z' and z_1 as the slab entrance (top) and exit (bottom) respectively (*cf.* Figure 1), and Fourier-transform equation (7) with respect to $\mathbf{x}_T$, resulting in

$$P(\mathbf{K}_T, z^*) = k^2 \int_{z'}^{z_1} dz \iint d^2\mathbf{x}_T g^0(\mathbf{K}_T, z^*; \mathbf{x}) F(\mathbf{x}) p^f(\mathbf{x}) \ , \tag{8}$$

where

$$g^0(\mathbf{K}_T, z^*; \mathbf{x}_T, z) = \frac{i}{2\gamma} e^{i\gamma|z^*-z|} e^{-i\mathbf{K}_T\cdot\mathbf{x}_T} \tag{9}$$

with

$$\gamma = \sqrt{k^2 - K_T^2} \ . \tag{10}$$

Substituting equation (9) into (8) yields

$$P(\mathbf{K}_T, z^*) = \frac{i}{2\gamma} k^2 \int_{z'}^{z_1} dz e^{i\gamma|z^*-z|} \iint d^2\mathbf{x}_T e^{-i\mathbf{K}_T\cdot\mathbf{x}_T} [F(\mathbf{x}_T, z) p^f(\mathbf{x}_T, z)] \ . \tag{11}$$

Note that the two dimensional inner integral is a 2-D Fourier transform. Therefore, the dual-domain technique can be used to implement equation (11).

2.4 The case of acoustic media

For a linear isotropic acoustic medium, the wave equation in frequency domain is

$$\nabla \cdot \frac{1}{\rho} \nabla p + \frac{\omega^2}{\kappa} p = 0 \ , \tag{12}$$

where p is the pressure field, ρ and κ are the density and bulk modulus of the medium, respectively.

Assuming ρ_0 and κ_0 as the parameters of the background medium, in the case of thin-slab and a constant medium, equation (12) can be written as

$$\frac{1}{\rho_0}\nabla^2 p + \frac{\omega^2}{\kappa_0} p = -[\omega^2(\frac{1}{\kappa} - \frac{1}{\kappa_0})p + \nabla \cdot (\frac{1}{\rho} - \frac{1}{\rho_0})\nabla p] \ , \tag{13}$$

or

$$(\nabla^2 + k^2)p(\mathbf{x}) = -k^2 F(\mathbf{x})p(\mathbf{x}) \ , \tag{14}$$

which has the same form as the case of scalar media except

$$F(\mathbf{x}) = \varepsilon_\kappa(\mathbf{x}) + \frac{1}{k^2}\nabla \cdot \varepsilon_\rho \nabla \ , \tag{15}$$

which is an operator instead of a scalar function, with

$$\varepsilon_\kappa(\mathbf{x}) = \frac{\kappa_0}{\kappa(\mathbf{x})} - 1 \ , \tag{16}$$

$$\varepsilon_\rho(\mathbf{x}) = \frac{\rho_0}{\rho(\mathbf{x})} - 1 \ . \tag{17}$$

If ρ keeps constant ($\rho = \rho_0$), then $\varepsilon_\kappa = c_0^2/c^2 - 1 = \varepsilon$, going back to the scalar medium case.

From equation (11), the dual-domain expression for scattered pressure field at the receiving depth z^* for acoustic media can be written explicitly as

$$P(\mathbf{K}_T, z^*) = \frac{i}{2\gamma}k^2 \int_{z'}^{z_1} dz e^{i\gamma|z^*-z|} \left\{ \int d^2\mathbf{x}_T e^{-i\mathbf{K}_T\cdot\mathbf{x}_T}[\varepsilon_\kappa(\mathbf{x}_T, z)p^f(\mathbf{x}_T, z)] \right.$$
$$\left. + \frac{i}{k}\hat{k} \cdot \int d^2\mathbf{x}_T e^{-i\mathbf{K}_T\cdot\mathbf{x}_T}[\varepsilon_\rho(\mathbf{x}_T, z)\nabla p^f(\mathbf{x}_T, z)] \right\} \ , \tag{18}$$

with

$$\hat{k} = \frac{1}{k}(\mathbf{K}_T, k_z) \ , \tag{19}$$

where $k_z = \pm\gamma$ for forescattering and backscattering, respectively. The incident field $p^f(\mathbf{x}_T, z)$ and its gradient $\nabla p^f(\mathbf{x}_T, z)$ at depth z can be calculated from the field at the slab entrance z', $p^0(\mathbf{x}'_T, z')$, as follows:

$$p^f(\mathbf{x}) = p^f(\mathbf{x}_T, z) = \frac{1}{4\pi^2}\iint d^2\mathbf{K}'_T p^0(\mathbf{K}'_T)e^{i\gamma'(z-z')}e^{i\mathbf{K}'_T\cdot\mathbf{x}_T} \tag{20}$$

and

$$\nabla p^f(\mathbf{x}) = \frac{ik}{4\pi^2}\iint d^2\mathbf{K}'_T \hat{k}' p^0(\mathbf{K}'_T)e^{i\gamma'(z-z')}e^{i\mathbf{K}'_T\cdot\mathbf{x}_T} \ , \tag{21}$$

where

$$\hat{k}' = \frac{1}{k}(\mathbf{K}'_T, \gamma') \ . \tag{22}$$

When the receiving level is at the bottom of the thin-slab (forescattering), $z^* = z_1$; while $z^* = z'$ is for the backscattered field at the top of the thin-slab. The total transmitted filed at the slab bottom can be calculated as the sum of the forescattered field and the primary field.

Note that equation (18) for calculating scattered fields does not involve any approximation except the dual-domain implementation (or split step algorithm). When the scales of heterogeneities in the medium are larger than the dominant wavelength, the method can be further approximated by using a screen scattering approximation which involves small-angle approximation to wave-medium interactions. The screen approximation can substantially reduce the computation time of the method. We will discuss its accuracy and limitations in future publications. In this paper we will concentrated on the wide-angle version of the method.

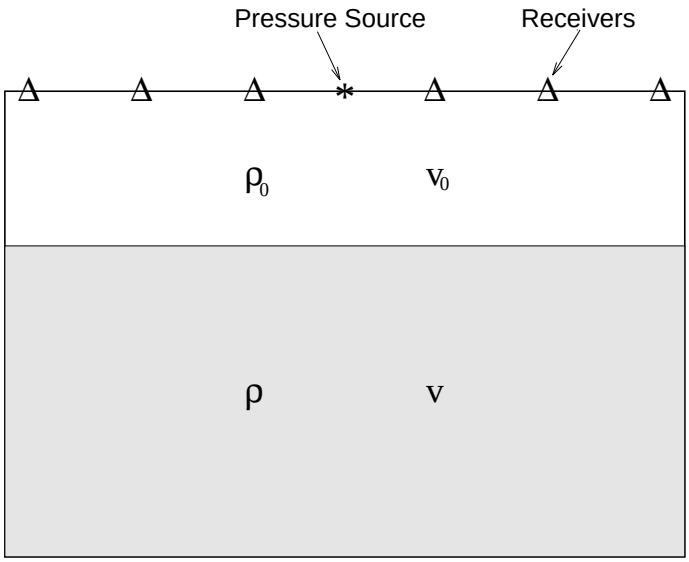

Figure 2: The schematic illustration for a 2-D layered model.

2.5 Implementation procedure

The procedure for calculating backscattered field in acoustic media can be summarized as follows. The simplification for the case of scalar media is straightforward.

1. Fourier transform the incident field at the entrance of each thin-slab into wavenumber domain.
2. Free propagation in wavenumber domain and calculate the primary field and its gradient within the slab.
3. At each depth within the slab, inverse FT the primary field and its gradient into space domain, and then interact with the medium perturbations: calculate the backscattered field.
4. FT the backscattered field into wavenumber domain and derive its divergence. Sum up scattered fields by bulk modulus and density, and multiply it with a weighting factor $i/(2\gamma)$. Then free propagate to the entrance of the slab. The total backscattered field by the thin-slab can be propagated to the surface using the multi-screen propagator.
5. Calculate the forescattered field at the slab exit and add it to the primary field to form the total field as the incident field at the entrance of the next thin-slab.
6. Continue the procedure iteratively.
7. Sum up all the backscattered waves to form the total scattered field at the surface.

3 NUMERICAL EXAMPLES

3.1 Reflection coefficients

We used a layered model defined on a 2048×300 rectangular grid (*cf.* Figure 2) to verify the ability of the proposed method for calculating reflected waves. In the model, the grid spacing in the horizontal direction is 8m and that in the vertical directions is 5m. The plane interface between the two layers is located at the depth of 500m. A pressure source with the first derivative of a Gaussian time history, a dominant frequency 20Hz and an amplitude 1.0 was introduced at the center of the upper border of the model. The velocity and density of the upper layer are 2000m/s and 1.0g/cm^3, respectively. Reflection coefficients at the interface were calculated for the different velocity and density perturbations in the lower layer using our proposed method. The frequency range used in the calculation is from 14.6Hz to 19.5Hz with 11 frequency components. We calculated reflection coefficients for

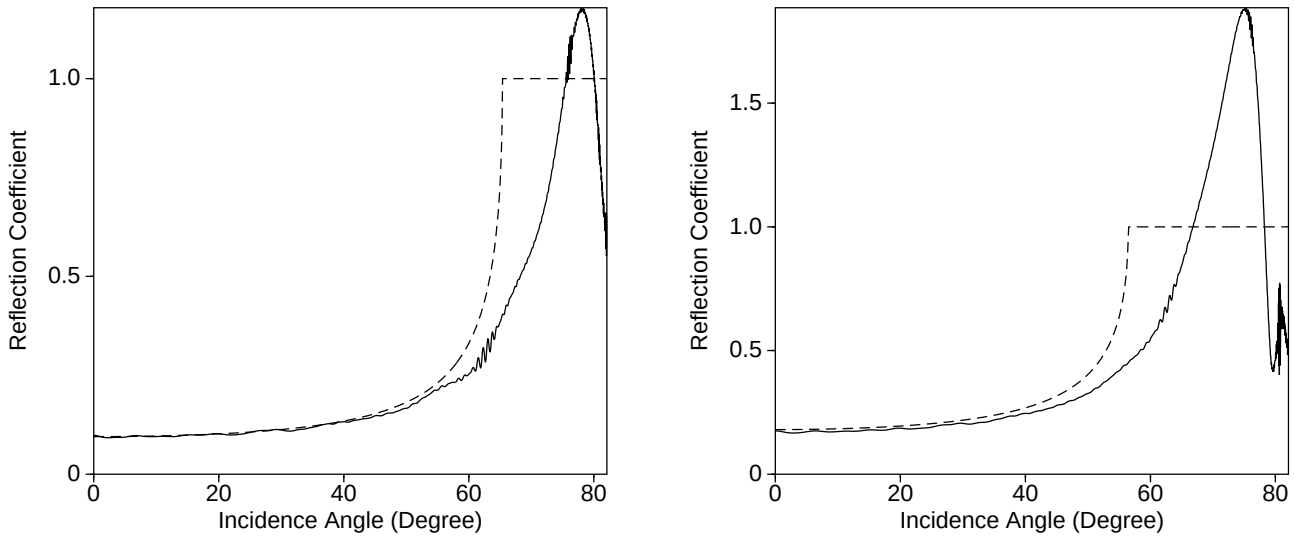

(a) (b)

Figure 3: Comparison between theoretical and simulated reflection coefficients of a high-velocity 'half-space' shown in Figure 2 when the velocity and density perturbations of the lower 'half-space' are (a) 10% and (b) 20%. Dashed lines represent the theoretical reflection coefficients and the solid curves, the simulated results.

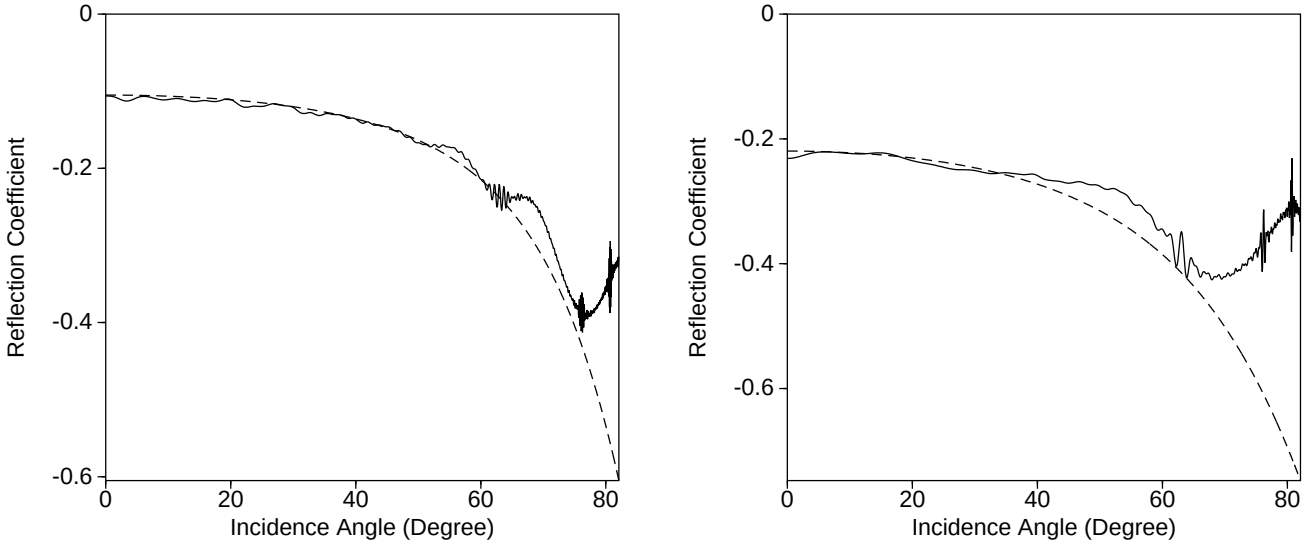

(a) (b)

Figure 4: Comparison between theoretical and simulated reflection coefficients of a low-velocity 'half-space' shown in Figure 2 when the velocity and density perturbations of the lower 'half-space' are (a) -10% and (b) -20%. Dashed lines represent the theoretical reflection coefficients and the solid curves, the simulated results.

each frequency component and took an average over the 11 frequencies (*cf.* Figure 3). Figure 3 (a) is the results for 10% of velocity and density perturbations in the lower layer and Figure 3 (b) is for 20%. In both figures, the dashed lines are theoretically predicted reflection coefficients of plane wave incidence and the solid curves are calculated results. These curves demonstrate that the calculated reflection coefficients are in good agreement with theoretical ones when the incidence angles are smaller than the critical angles. When the incidence angles are near and beyond the critical angles, the numerical results deviate from the theoretical curves. This may be due to several reasons such as the curved wavefronts of waves from the point source, the wavenumber filtering in the process of forward propagation which reduces the amplitudes of large-angle scattered waves, and the effect of finite layer thickness. The amplitudes of the calculated reflection coefficients decrease when the incidence angles are larger than approximately 70° due to the wavenumber filtering during the calculation of forward propagation.

When the velocity and density perturbations of the lower layer are -10% and -20%, the corresponding results are given in Figure 4 (a) and (b), respectively. For Figure 4 (a), the frequency range is the same as above while the frequency range is from 4.88Hz to 9.77Hz with 11 frequency components for Figure 4 b. We see from these figures that calculated reflection coefficients agree well with the theoretical results when the incidence angles are smaller than approximately 70°. For larger incidence angles, the amplitudes of reflection coefficients decrease because of the wavenumber filtering.

3.2 Synthetic seismograms of reflected waves

The model shown in Figure 2 was used for the simulations of reflected waves from the two plane interfaces in the model. Both the grid spacings in the horizontal and vertical directions are 5m. The velocity and density of the upper layer are 4000m/s and 1.0g/cm^3, respectively. For the first simulation, the velocity of the lower layer is 4400m/s and the density is kept the same as the upper layer. For the second simulation, the density of the lower layer is set to be 1.1g/cm^3 while the velocity is reduced so that the bulk modulus of this layer is kept the same as that in the first simulation. Therefore, the velocity of the lower layer becomes 4195.2m/s. The pressure source introduced at the center of the upper border of the model is a Ricker's time history with a dominant frequency 10Hz and an amplitude 1.0. Receivers were located at the grid points at the surface. Computations were made for 1024 time steps using a vertical space interval of 20m for the phase-screen propagator. The time interval is 0.004s. Figure 5 (a) and (b) depict respectively the central part of seismograms (*i.e.* reflected pressure fields) recorded at the receivers for both simulations. We see from Figure 5 (b) that the reflected waves from the lower border of the model arrive at a later time than that in Figure 5 (a) and that the amplitudes of reflected waves are larger than those in Figure 5 (a), as expected.

Next, we present an example of simulation of reflected waves from a cylindrical heterogeneous body located at the center of a homogeneous model defined on a 2048×400 grid (*cf.* Figure 6). The grid spacings are the same as above. The diameter of the cylindrical body is 1000m. The velocity and density of the background medium are 4000m/s and 1.0g/cm^3, respectively. The velocity and density of the cylindrical heterogeneous body are the same as those of the lower layer of the above model. Other parameters are the same as above. The same computations as above were made for 1024 time steps and the corresponding seismograms are given in Figure 7. Comparing Figure 7 (a) and (b), we can see the differences between them similar to those between Figure 5 (a) and (b).

4 CONCLUSIONS AND DISCUSSION

We have developed a fast dual-domain method for modeling reflected waves in heterogeneous acoustic media based on the De Wolf approximation, *i.e.* the multiple-forescattering single-backscattering approximation. It can handle wide-angle scattering. The computation speed of the method would be much faster than classical full wave finite difference approaches because of the one-way propagation features and the usage of FFT in our method. Therefore, the method is very suitable for large 3-D modeling, migration/inversion problems.

Numerical examples showed that the relection coefficients of a plane interface derived from numerical simulations by our method match the theoretical curves well up to critical angles. The proposed method can even model the critical and post-critical reflections with the correct phase and travel times, although the amplitudes may deviate from the ideal plane wave reflections. In the numerical examples presented in this paper, the magnitude of simulated reflection coefficients fall off from the theoretical curves beyond about 70°. This may be further

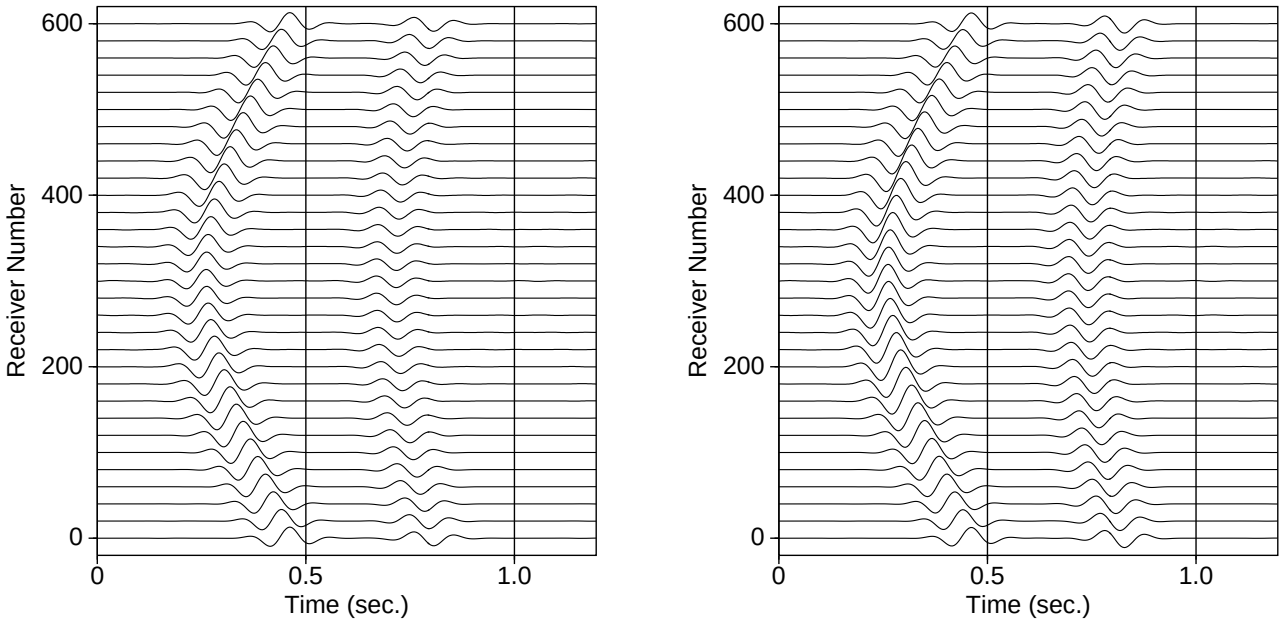

Figure 5: Seismograms recorded during the simulations of reflected waves from a layered model (*cf.* Figure 2). (a) is for the case where the densities of the upper and lower layers are the same while their velocities are different. (b) is for the case where the density and velocity of the lower layer are both different from those of the upper layer. The same scale was used in (a) and (b).

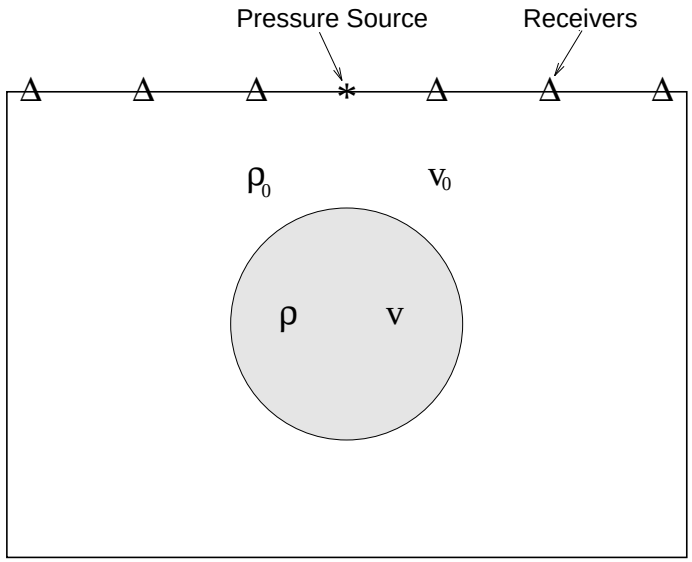

Figure 6: The schematic illustration for a 2-D model with a cylindrical heterogeneous body at the center of the model.

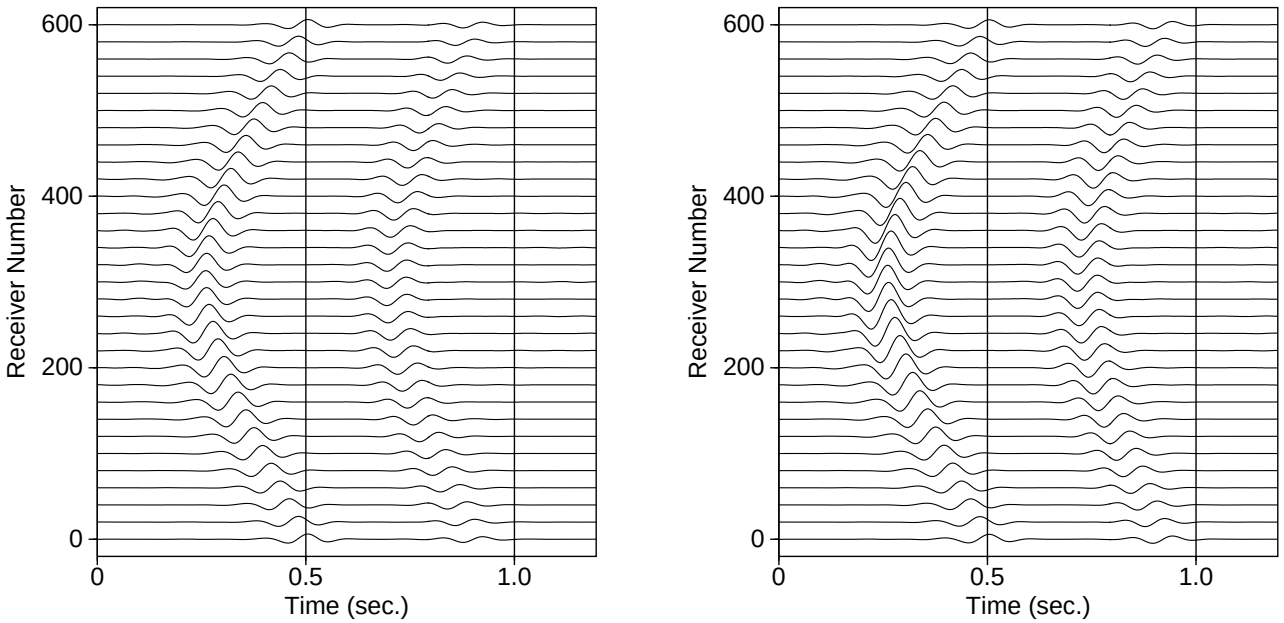

Figure 7: Seismograms recorded during the simulations of reflected waves from the model shown in Figure 6. (a) is for the case where the densities of the cylindrical heterogeneous body and background medium are the same while their velocities are different. (b) is for the case where the density and velocity of the cylindrical heterogeneous body are both different from those of the background medium. The same scale was used in (a) and (b).

improved by optimizing the wavenumber filtering in our algorithm and decreasing the marching step length in z-direction. From the derivation of the method based on a perturbation approach and a dual-domain implementation, we understand that the method has an accurate implementation for the horizontal Helmholtz operator, but retains as a first order finite difference algorithm in z-direction. Therefore, the errors of the algorithm depend on the step length in z-direction, heterogeneity strength and the spectral properties of the heterogeneities. Detailed study of the method for 3-D cases and comparisons with finite difference methods including accuracy and computation speed will be given in the future publications.

ACKNOWLEDGEMENTS

The authors would like to thank X.B. Xie for the discussion and his help in many aspects. The work was supported by a grant from the Los Alamos National Laboratory Institutional Supported Program, under the auspices of the United States Department of Energy, and by the Airforce Office of Scientific Research through contract F49620-95-1-0028 administered by the Phillips Laboratory of the Air Force. The support from the W.M. Keck Foundation is also acknowledged. Institute of Tectonics, University of California, contribution 275.

References

[1] Beydoun, W.B. and Mendes, M., 1989. Elastic ray-Born ℓ_2-migration/inversion, *Geophys. J. Int.*, **97**, 151-160.

[2] Červený, V., 1981. Seismic wave fields in structurally complicated media (Ray and Gaussian beam approaches), Lecture Notes, Rijksuniversiteit Utrecht, Vening-Meinesz Laboratory, Utrecht.

[3] Červený, V. and Klimeš, L., 1984. Synthetic body wave seismograms for three-dimensional laterally varying media, *Geophys. J. Int.*, **79**, 119-133.

[4] Chapman, C.H., 1985. Ray theory and its extensions: WKBJ and Maslov seismograms, *J. Geophys.*, **58**, 27-43.

[5] Coates, R.T. and Chapman, C.H., 1990. Ray perturbation theory and the Born approximation, *Geophys. J. Int.*, **100**, 379-392.

[6] Coates, R.T. and Chapman, C.H., 1991. Generalized Born scattering of elastic waves in 3-D media, *Geophys. J. Int.*, **107**, 231-263.

[7] De Wolf, D.A., 1971. Electromagnetic reflection from an extended turbulent medium: cumulative forward-scatter single-backscatter approximation, *IEEE trans. Ant. and Propag.*, **AP-19**, 254-262.

[8] De Wolf, D.A., 1985. Renormalization of EM fields in application to large-angle scattering from randomly continuous media and sparse particle distributions, *IEEE trans. Ant. and Propag.*, **AP-33**, 608-615.

[9] Gubernatis, J.E., Domany, E., Krumhansl, J.A. and Huberman, M., 1977. The Born approximation in the theory of the scattering of elastic waves by flaws, *J. Appl. Phys.*, **48**, 2812-2819.

[10] Martin, J.M. and Flatté, S.M., 1988. Intensity images and statistics from numerical simulation of wave propagation in 2-D random media, *Appl. Opt.*, **17**, 2111-2126.

[11] Stoffa, P.L., Fokkema J.T., Freire, R.M.D., and Kessinger, W.P., 1990. Split-step Fourier migration, *Geophysics*, **55**, 410-421.

[12] Thomson, D.J. and Chapman, N.R., 1983. A wide-angle split-step algorithm for the parabolic equation, *J. Acoust. Soc. Am.*, **74**, 1848-1854.

[13] Wu, R.S., 1994. Wide-angle elastic wave one-way propagation in heterogeneous media and an elastic wave complex-screen method, *J. Geophys. Res.*, **99**, 751-766.

[14] Wu, R.S. and Aki, K., 1985. Scattering characteristics of waves by an elastic heterogeneity, *Geophysics*, **50**, 582-595.

[15] Wu, R.S. and Huang, L.J., 1992. Scattered field calculation in heterogeneous media using a phase-screen propagator, *Expanded Abstracts of the Technical Program, SEG 62th Annual Meeting*, 1289-1292.

[16] Wu, R.S., Huang, L.J., and Xie, X.B., 1995. Backscattered wave calculation using the De Wolf approximation and a phase-screen propagator, submitted to *Expanded Abstracts of the Technical Program, SEG 65th Annual Meeting.*

[17] Xie, X.B. and Wu, R.S., 1995. A complex-screen method for modeling elastic wave reflections, submitted to *Expanded Abstracts of the Technical Program, SEG 65th Annual Meeting.*